DR | STUR
ENGINEERING | CONSULTING

DR. STUR
ENGINEERING CONSULTING

MILDRED-SCHEEL-BOGEN 12
80804 MÜNCHEN
GERMANY

PHONE: +49 (0) 89 / 200 90 267
MOBILE: +49 (0) 173 / 57 28 624

STEPHAN@STUR.DE

Test Report

Report No.: ZIR-141120-rev0

Date: 22-May-2015

Test specimen:

Ceramic Dental Implants

Test method:

Finite Element Analysis

Customer:

ZIRKONUS Implantatsysteme
Sotiris Suck
Heerweg 15 D
73770 Denkendorf
GERMANY

Examiner:

Dr. Stur Engineering Consulting
Dr.-Ing. Stephan Stur
Mildred-Scheel-Bogen 12
80804 München
GERMANY

Signature: S. Stur ______________________________
Dr. Stephan Stur

Notice:
The test results relate only to the items tested!

1 Subcontractors

None

2 Specimens

Ceramic Dental Implants:

Model 1 (no cement):
Original CAD file name: 'bg_impl_small_l14.stp', received 20-Nov-2014

Model 2 (with cement):
Original CAD file name: 'implantat_small_l14.stp', received 18-Dec-2014

Model 3 (with cement):
Original CAD file name: 'implantat_small_l14.stp', received 17-Apr-2015

3 Objective

The objective of the examination is the determination of the static stress values in three dental implant systems with no pre-angled connecting parts using Finite Element Analysis. Set-up and loading conditions of the dental implant system were realized according to ISO 14801 (2007).

Fig. 1 shows the three CAD models of the implant systems examined (full model and cross-section). Model 2 and model 3 contain an additional cement layer between the cap (loading member) and the implant body.

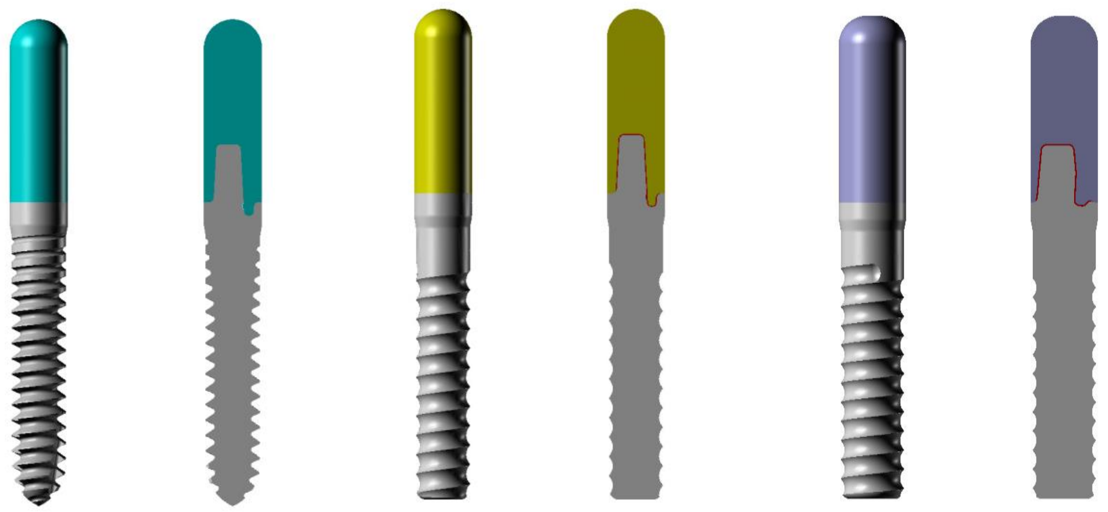

Fig. 1: CAD models of the implant systems: Model 1 (left), model 2 (center) and model 3 (right).

4 Test Procedure

4.1 Model description

4.1.1 Test setups

Finite Element Analysis (FEA) has been used to examine three different dental implant systems. Three-dimensional FE model were used to simulate the setup and loading conditions according to ISO 14801 (2007). Fig. 2 shows the set-up for non pre-angled connecting parts as is the case with the examined implant systems.

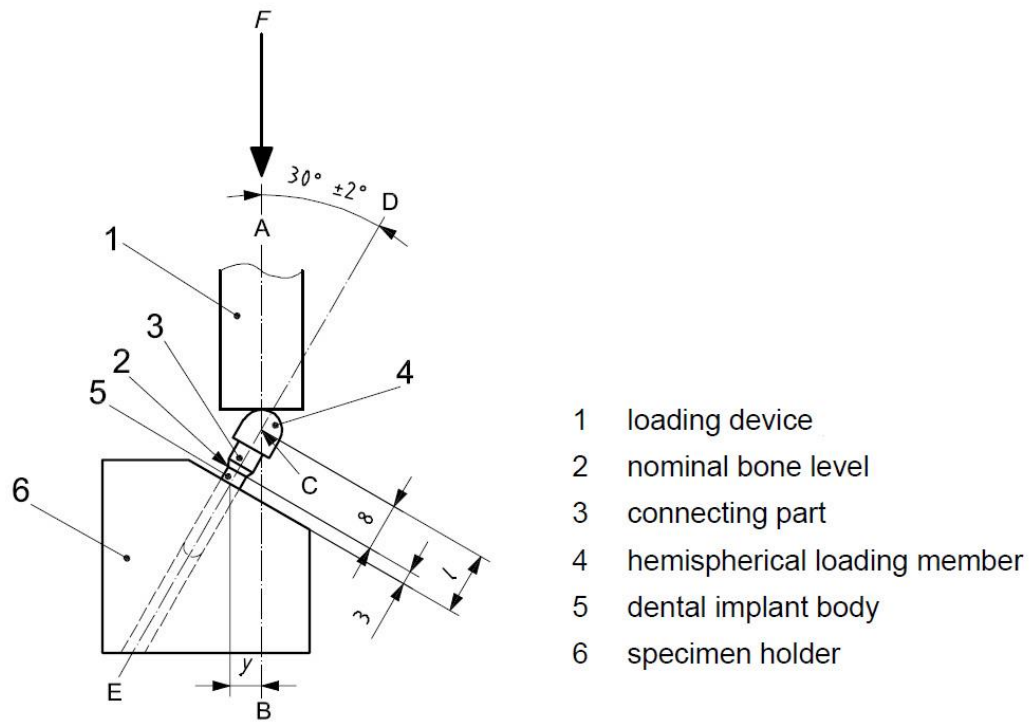

Fig. 2: Test setup for non pre-angled connecting parts according to ISO 14801 (2007).

Fig. 3 shows the test set-up realized in the FE models. A vertical load of 200 N was applied to the models. The implant is embedded in a bone layer and the embedding is fixed against movement. The upper end of the embedding is 3.0 mm apically from the nominal bone level to simulate the scenario according to the ISO standard.

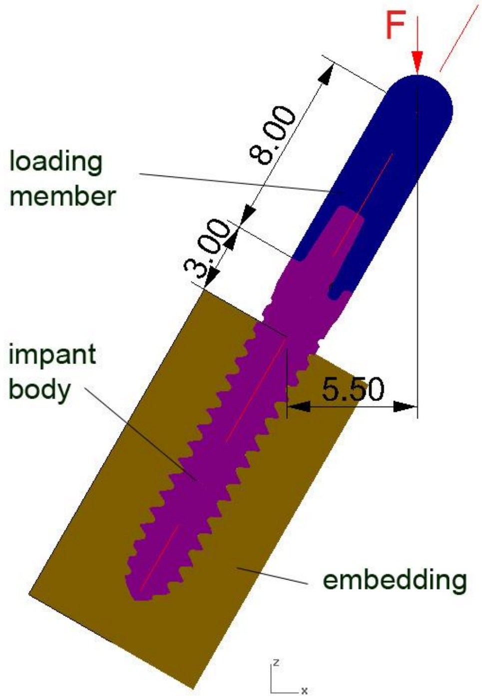

Fig. 3: Test setup for the FE simulations (model 1).

4.2 Test Equipment

The FE simulations were carried out using the FE program MSC.MARC 2014, for pre- and post-processing the program MSC.MENTAT 2014 (both MSC.Software, Santa Ana, CA, USA) was used.

4.3 Test Description

4.3.1 Material properties

Tab. 1 shows the properties of the materials used in the FE simulations.

Tab. 1: Material properties of the components.

Component	Material	Young's modulus	Poisson ratio
Loading member	Zirconia	210 GPa	0.33
Implant body	Zirconia	210 GPa	0.33
Embedding	Bone layer	6 GPa	0.30
Dental cement	Glass Ionomer Cement	4 GPa	0.42

4.3.2 FE models

The FE meshes consist of three-dimensional tetrahedral elements with isotropic elastic material behavior. In the FE models second order 10-node tetrahedron elements with improved bending characteristics are used.

Fig. 4 to Fig. 12 show the three-dimensional meshes of embedding, implant and loading member for all models. The elements of the cement layers are highlighted.

In model 1 between the loading member and the implant body and between implant body and the embedding a fixed connection (‘glued contact’) was modeled. In model 2 and model 3 the fixed connection was used between all components apart from the couple *implant body / loading member* where contact with possible separation was modeled.

For model 2 an additional setup was used with an inclination of the implant assembly of -30° instead of +30° as shown in Fig. 2 and Fig. 3.

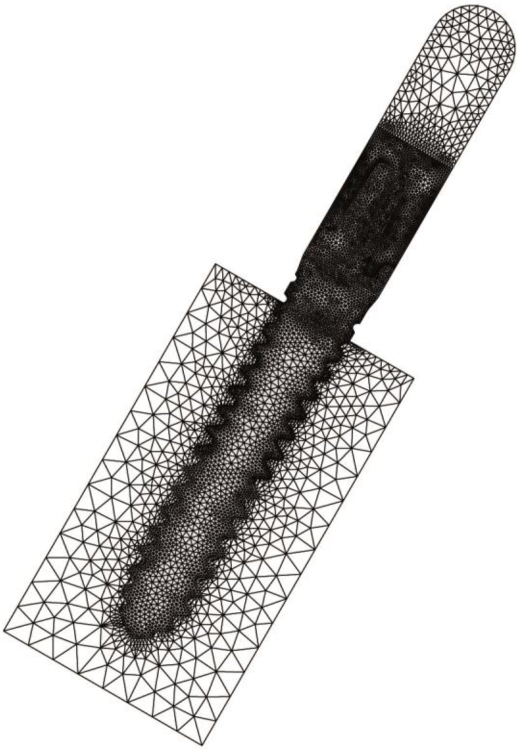

Fig. 4: FE mesh of the dental implant assembly of model 1 (701594 elements, 640743 nodes).

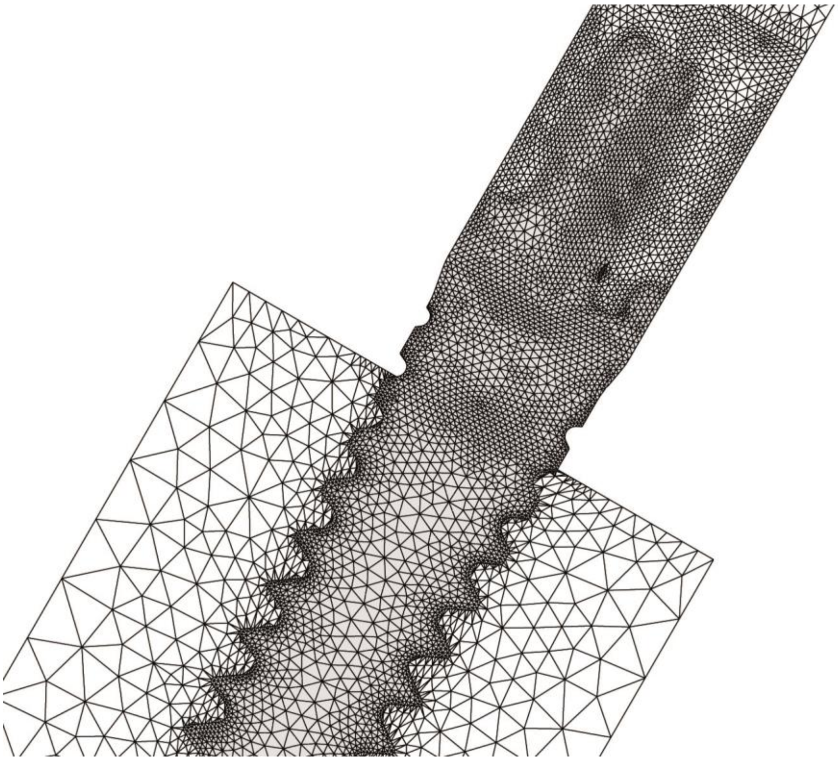

Fig. 5: Detail of Fig. 4.

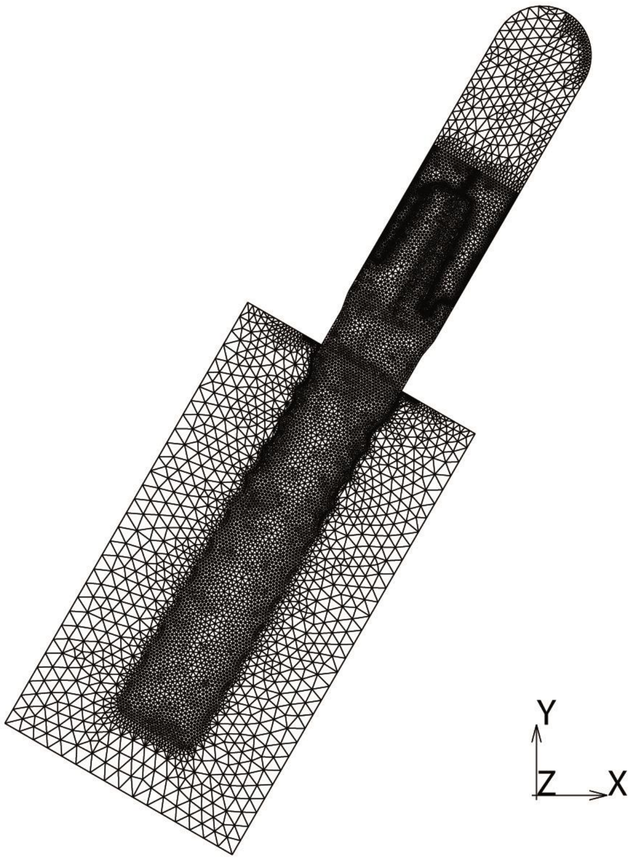

Fig. 6: FE mesh of the dental implant assembly of model 2 (+30°) (774327 elements, 750130 nodes).

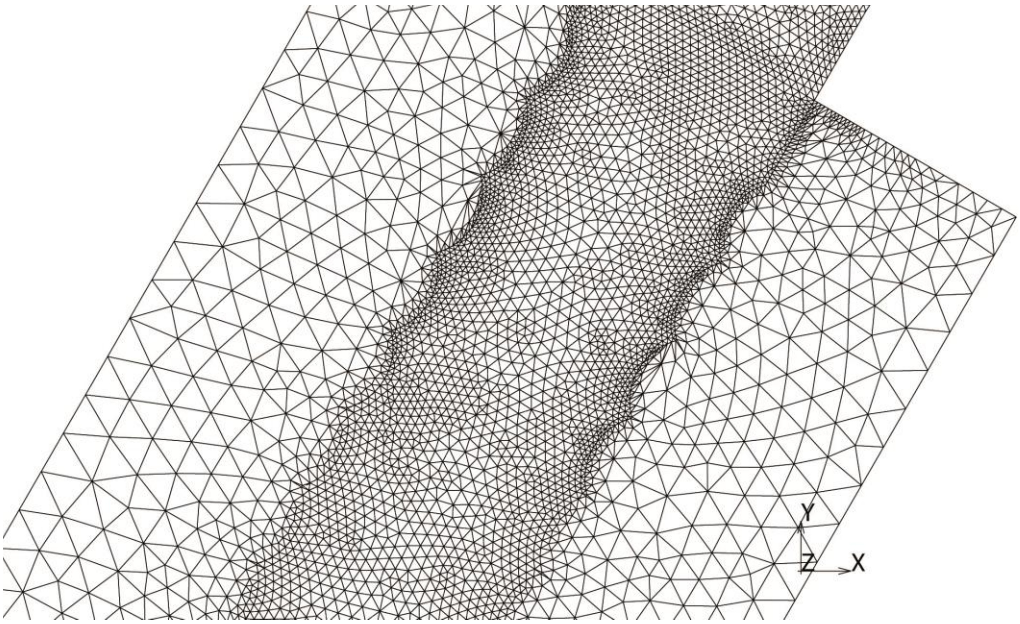

Fig. 7: Detail of Fig. 6.

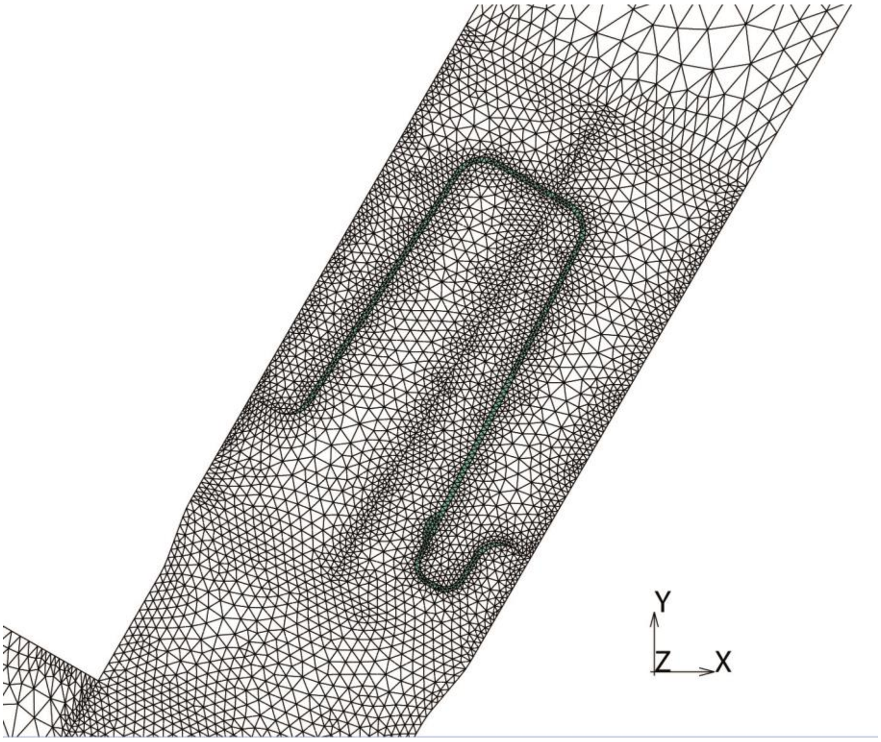

Fig. 8: Detail of Fig. 6.

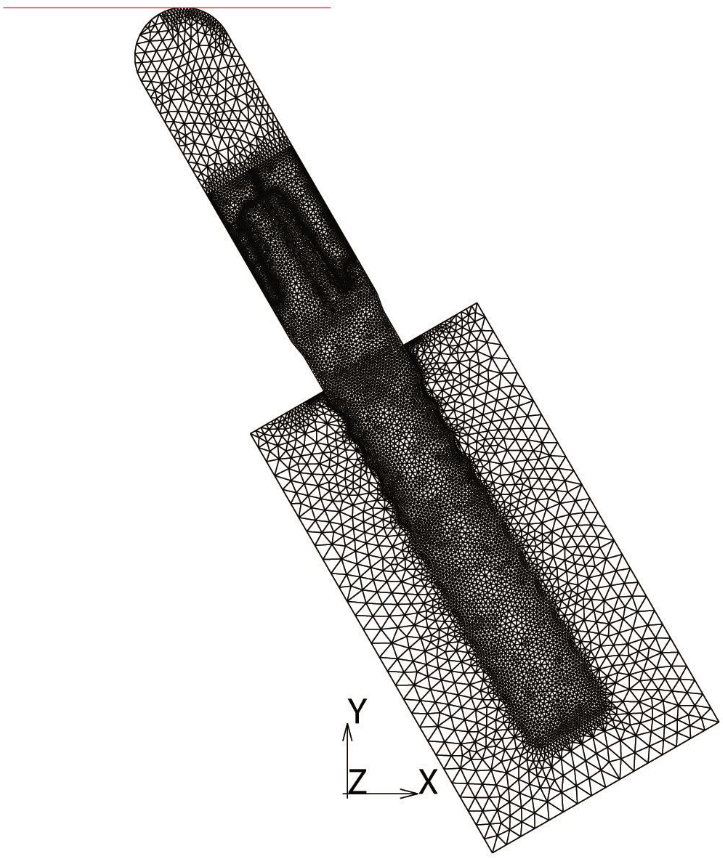

Fig. 9: FE mesh of the dental implant assembly of model 2 (-30°) (774327 elements, 750130 nodes).

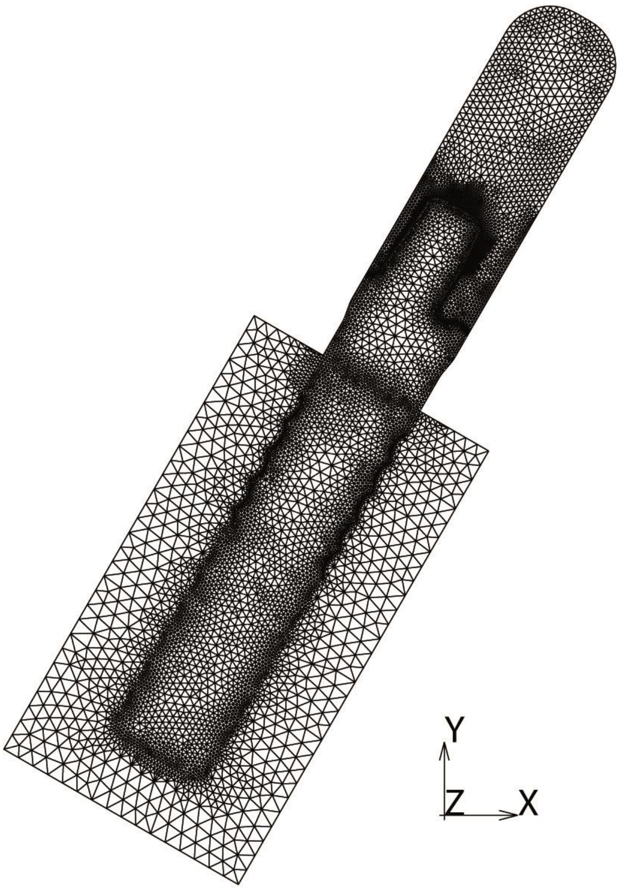

Fig. 10: FE mesh of the dental implant assembly of model 3 (717541 elements, 754493 nodes).

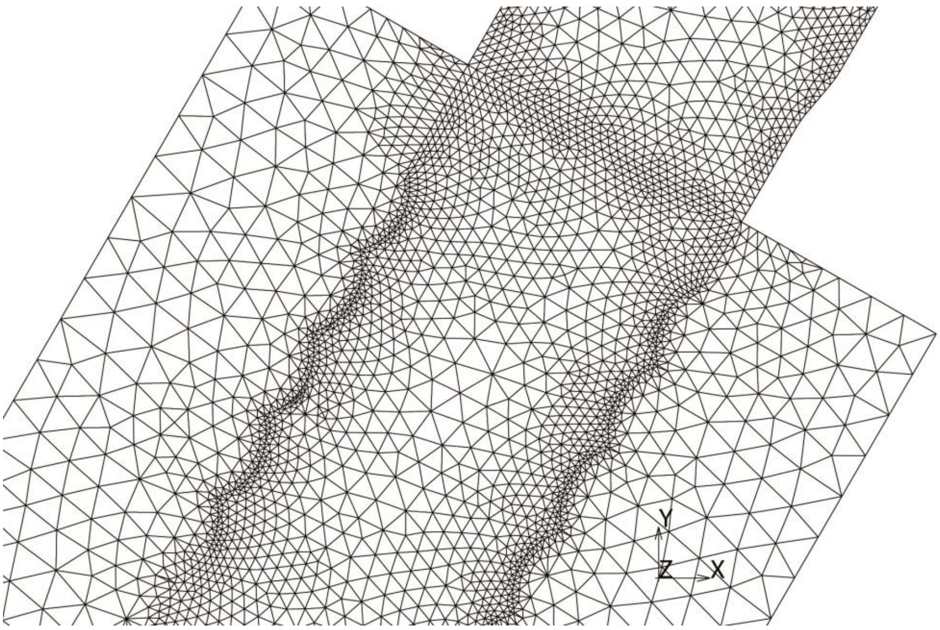

Fig. 11: Detail of Fig. 10.

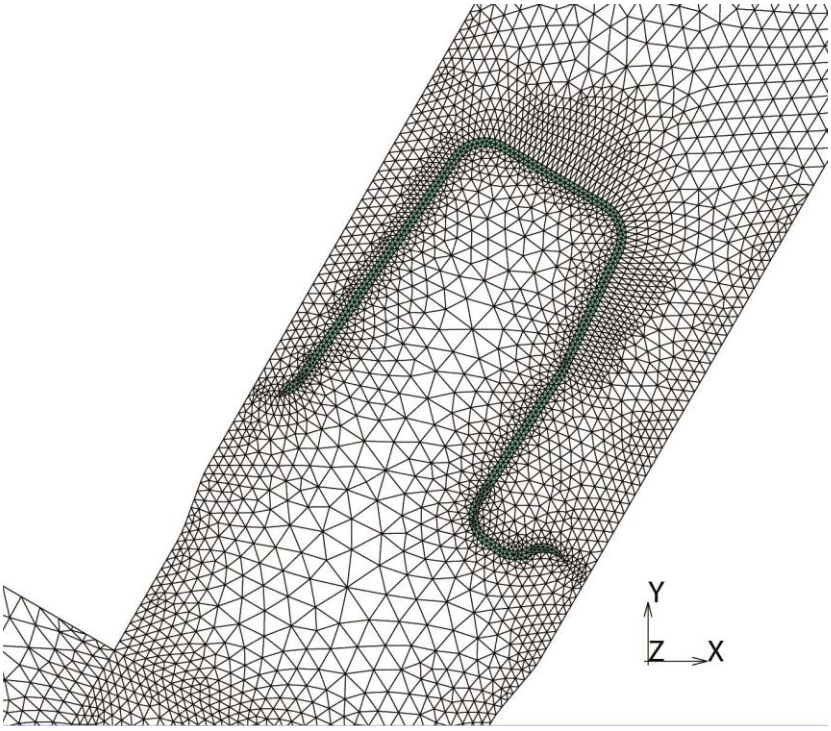

Fig. 12: Detail of Fig. 10.

5 Results

Tab. 2 shows the maximum principal stresses in the implant bodies of all models under the vertical load application of 200 N.

Tab. 2: Maximum tensile principal stress values.

Model	Max. principal stress
Model 1 (+30°)	1519 MPa
Model 2 (+30°)	1178 MPa
Model 2 (-30°)	959 MPa
Model 3 (+30°)	560 MPa

Model 1 (+30°): Vertical load 200 N

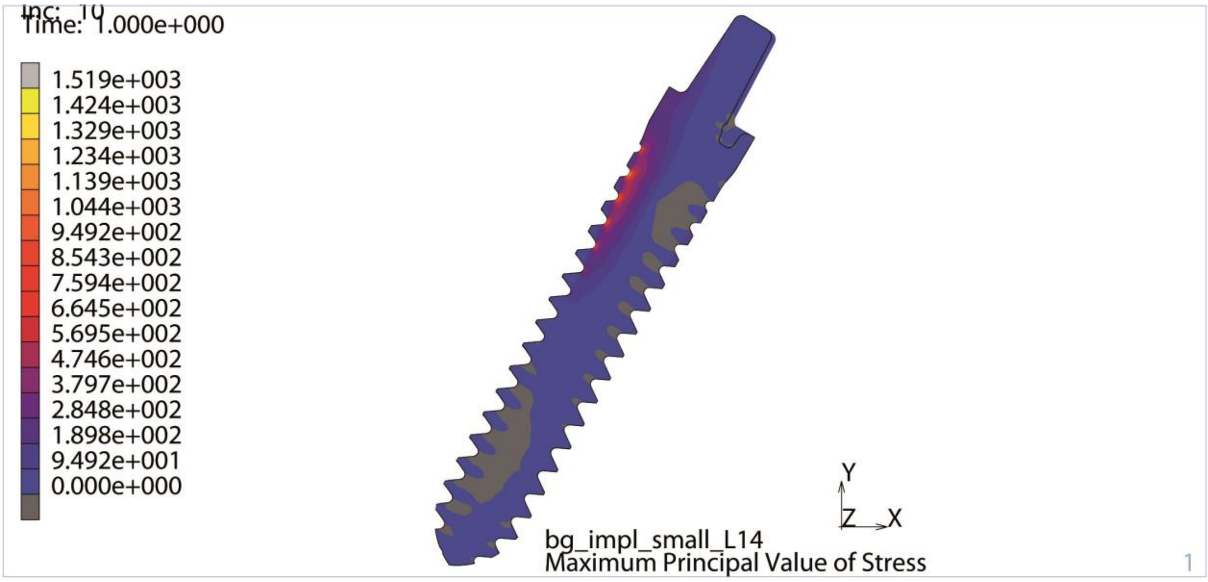

Fig. 13: Model 1 (+30°), load 200 N: Maximum principal stresses [MPa].

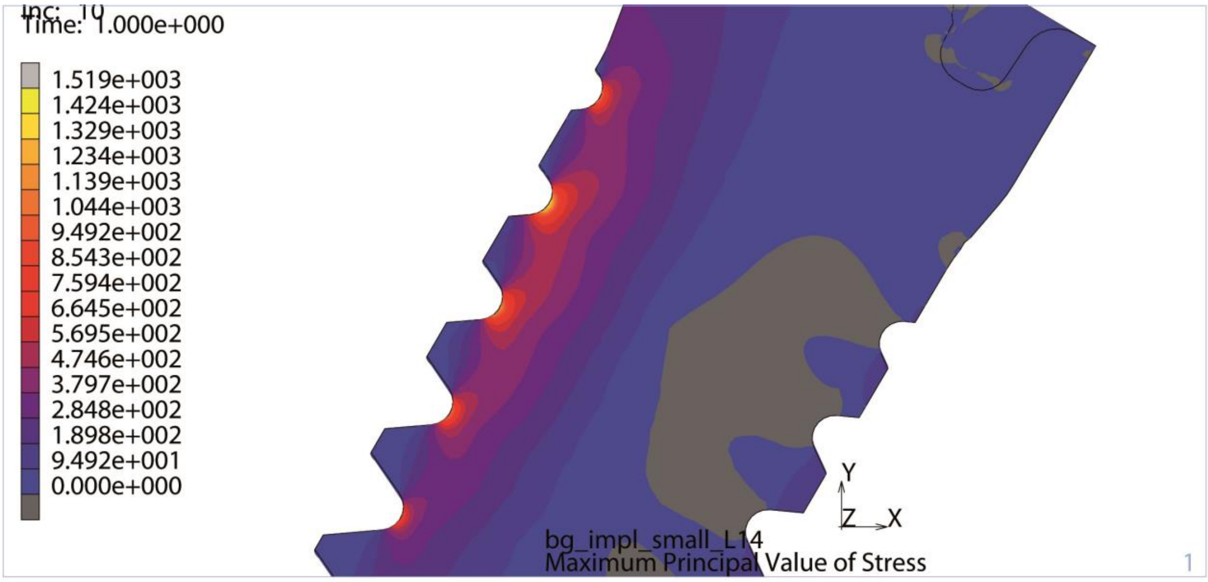

Fig. 14: Model 1 (+30°), load 200 N: Maximum principal stresses [MPa].

Model 1 (+30°): Vertical load 200 N

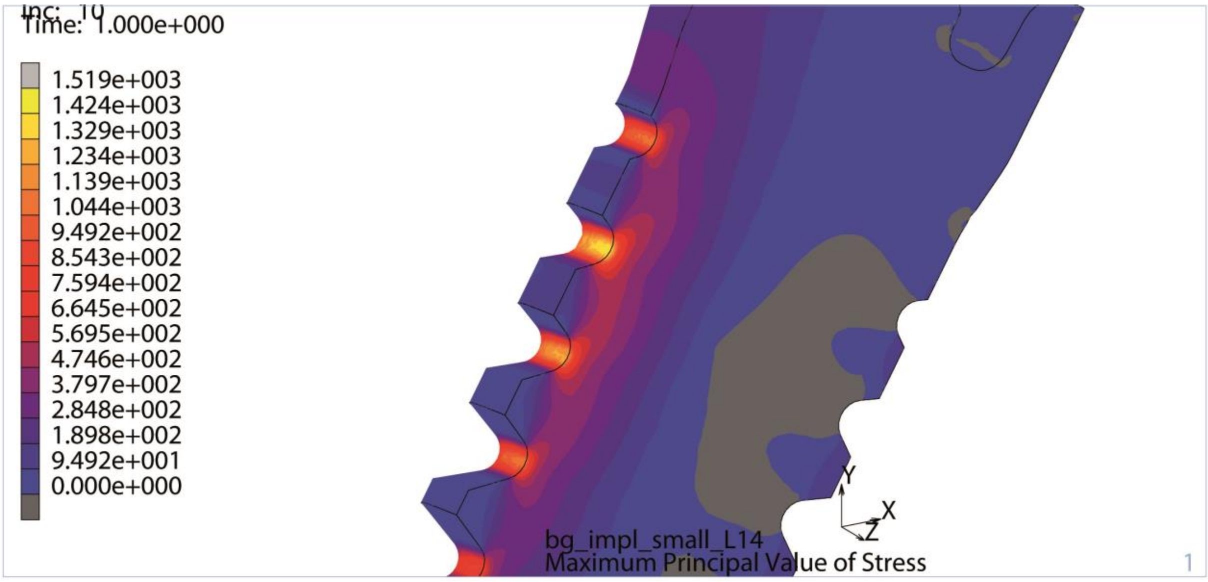

Fig. 15: Model 1 (+30°), load 200 N: Maximum principal stresses [MPa].

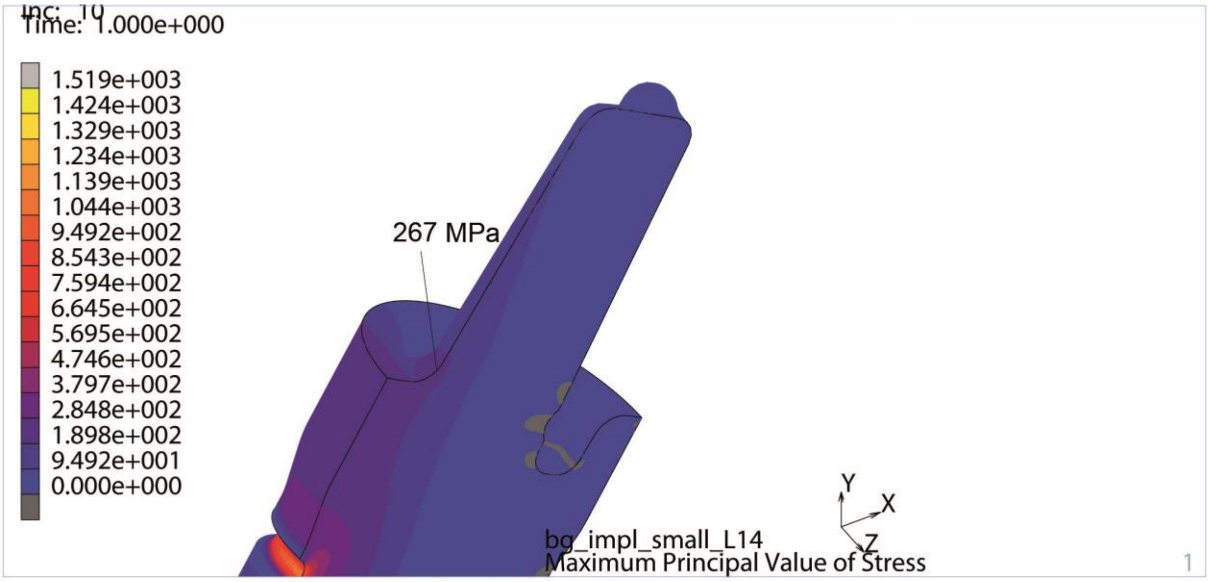

Fig. 16: Model 1 (+30°), load 200 N: Maximum principal stresses [MPa].

Model 2 (+30°): Vertical load 200 N

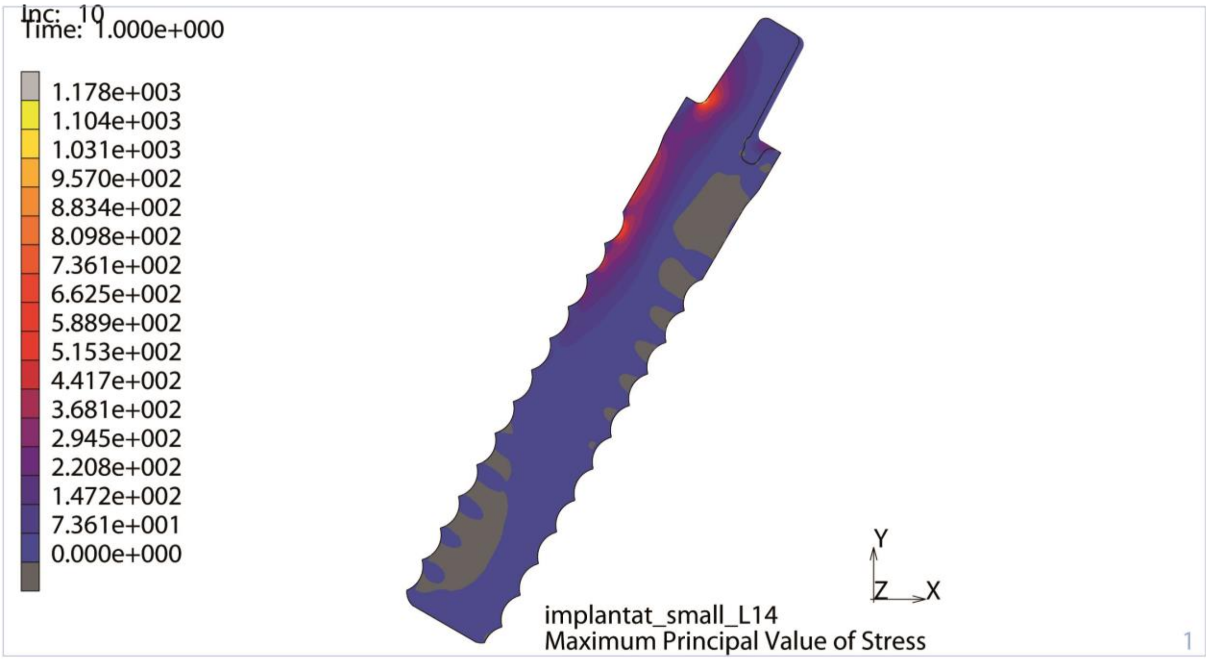

Fig. 17: Model 2 (+30°), load 200 N: Maximum principal stresses [MPa].

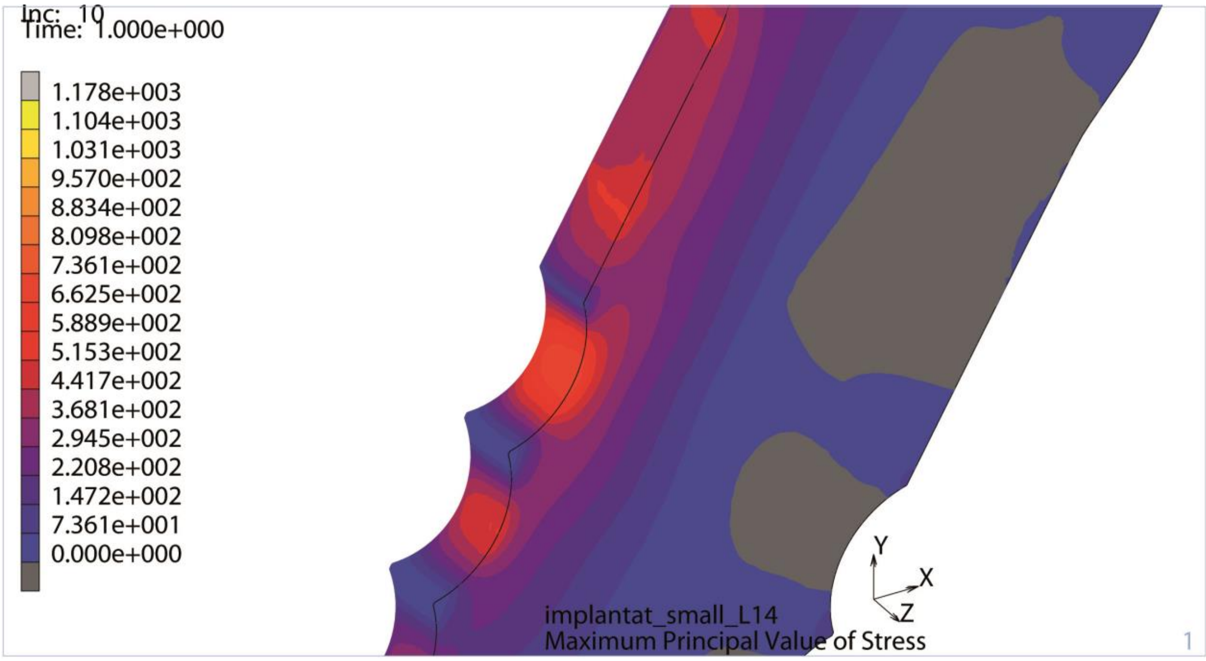

Fig. 18: Model 2 (+30°), load 200 N: Maximum principal stresses [MPa].

Model 2 (+30°): Vertical load 200 N

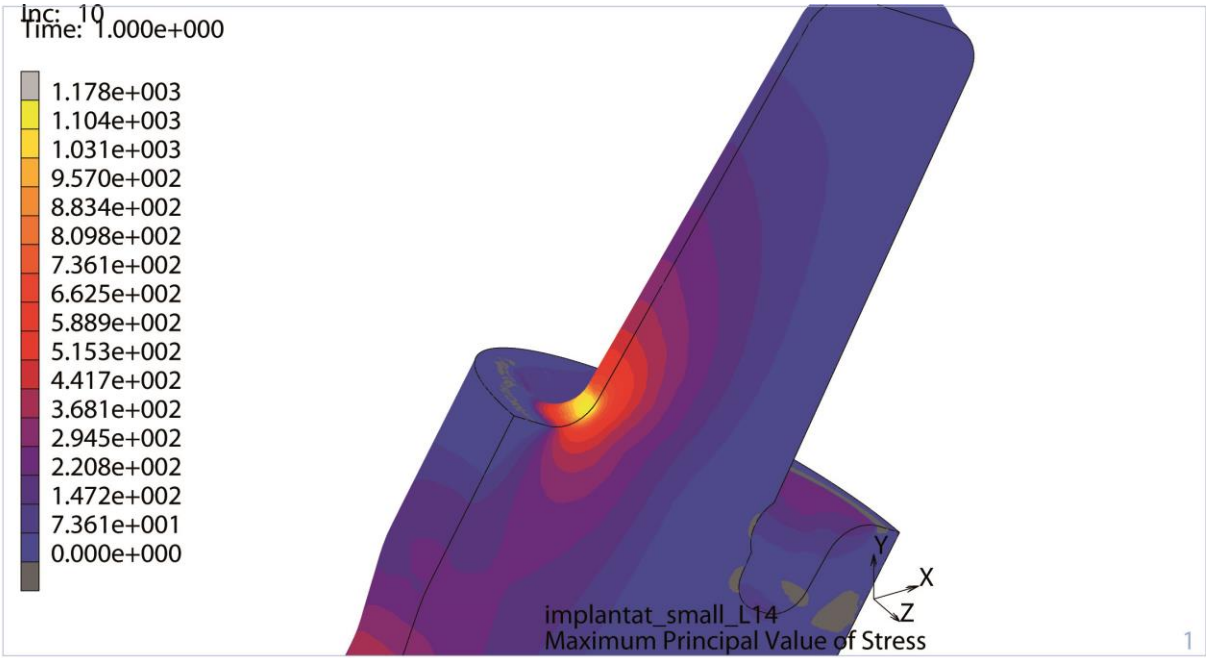

Fig. 19: Model 2 (+30°), load 200 N: Maximum principal stresses [MPa].

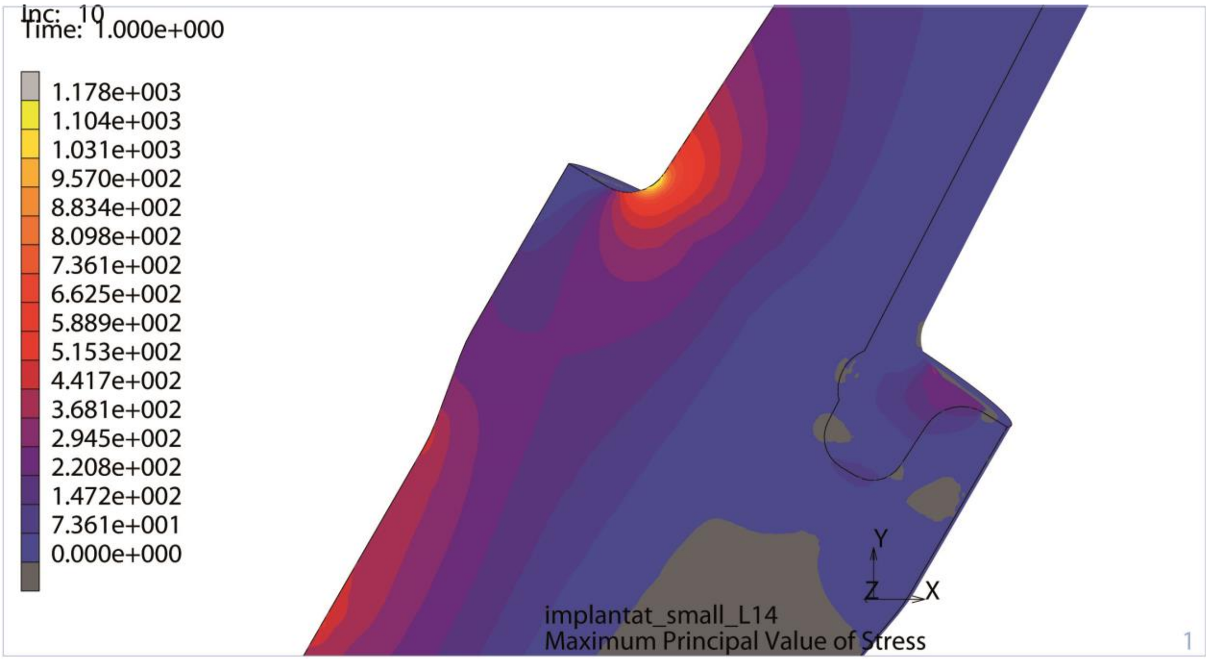

Fig. 20: Model 2 (+30°), load 200 N: Maximum principal stresses [MPa].

Model 2 (+30°): Vertical load 200 N

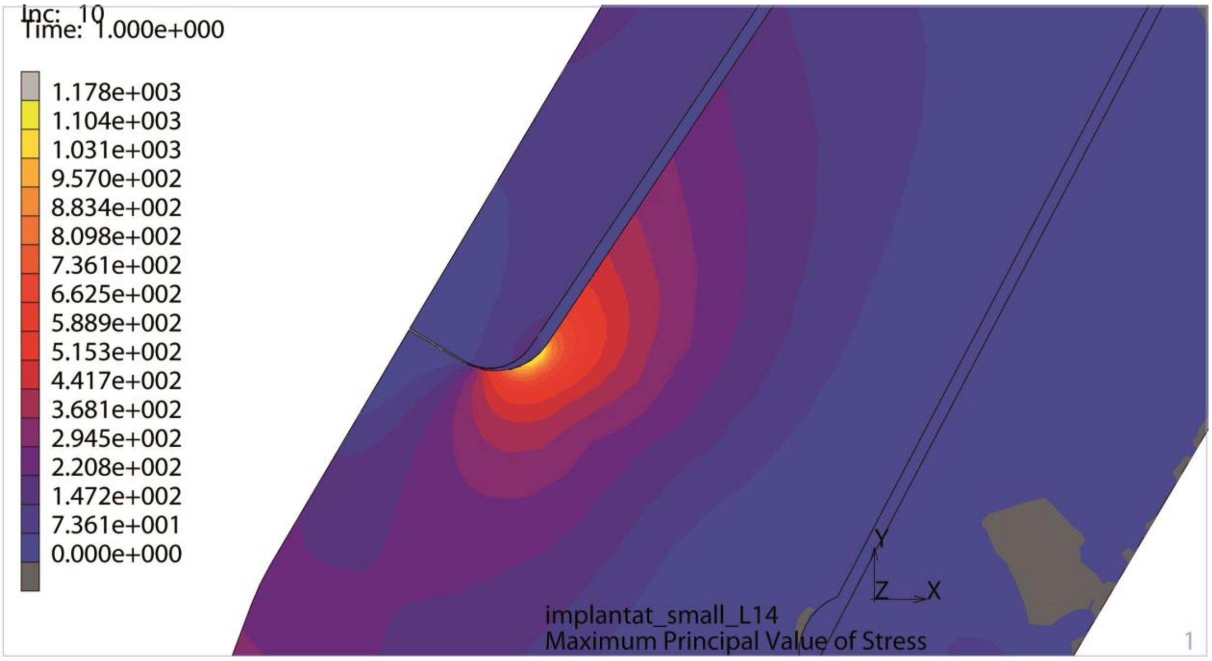

Fig. 21: Model 2 (+30°), load 200 N: Maximum principal stresses [MPa].

Model 2 (-30°): Vertical load 200 N

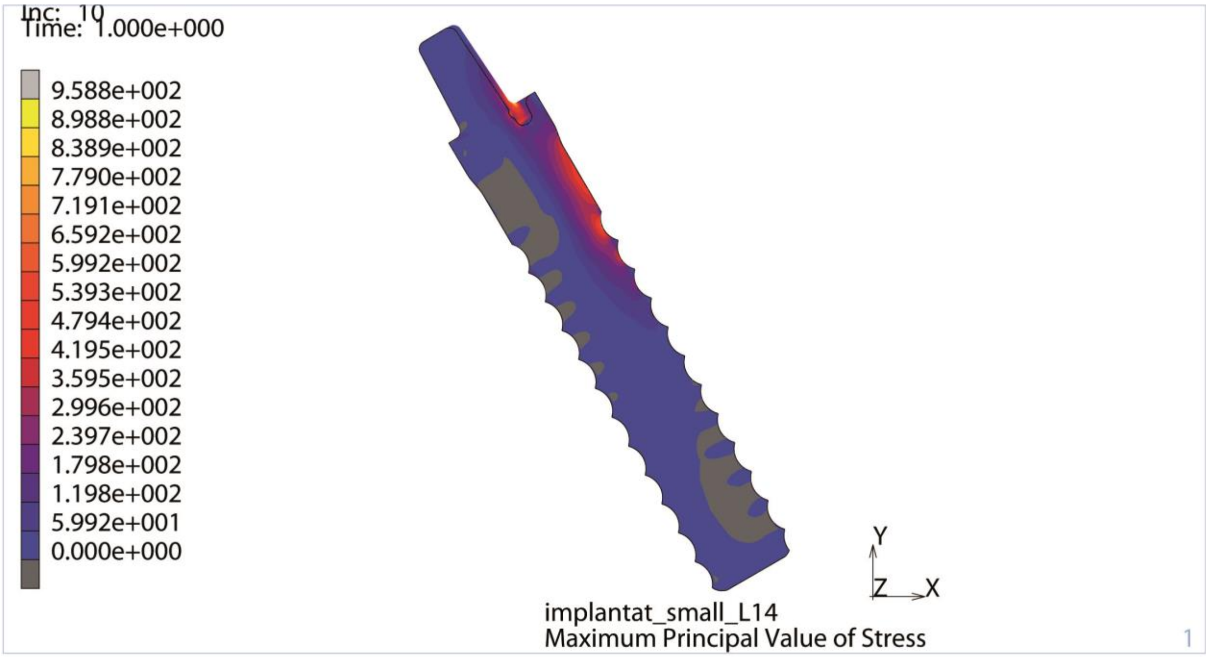

Fig. 22: Model 2 (-30°), load 200 N: Maximum principal stresses [MPa].

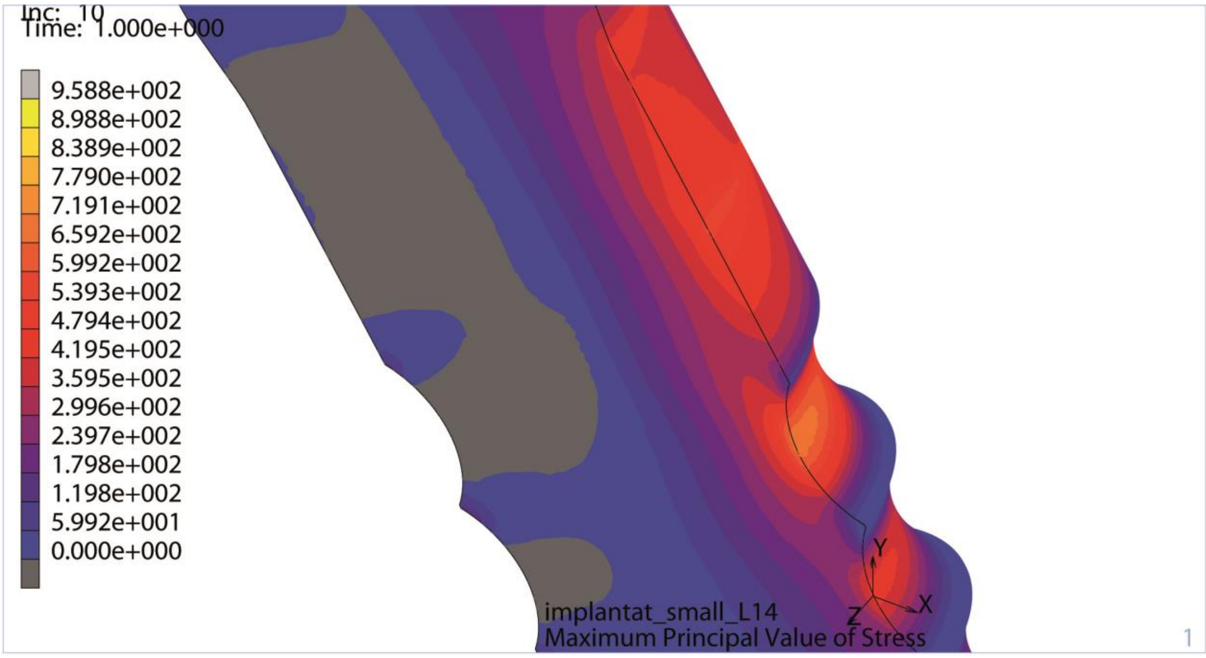

Fig. 23: Model 2 (-30°), load 200 N: Maximum principal stresses [MPa].

Model 2 (-30°): Vertical load 200 N

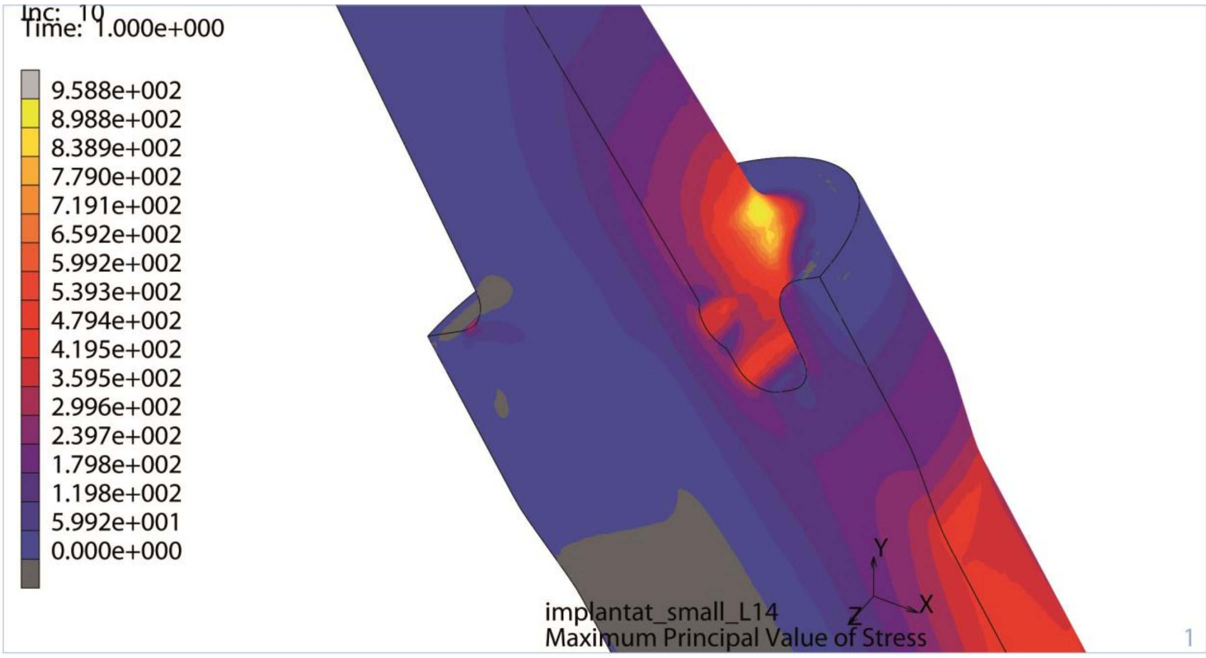

Fig. 24: Model 2 (-30°), load 200 N: Maximum principal stresses [MPa].

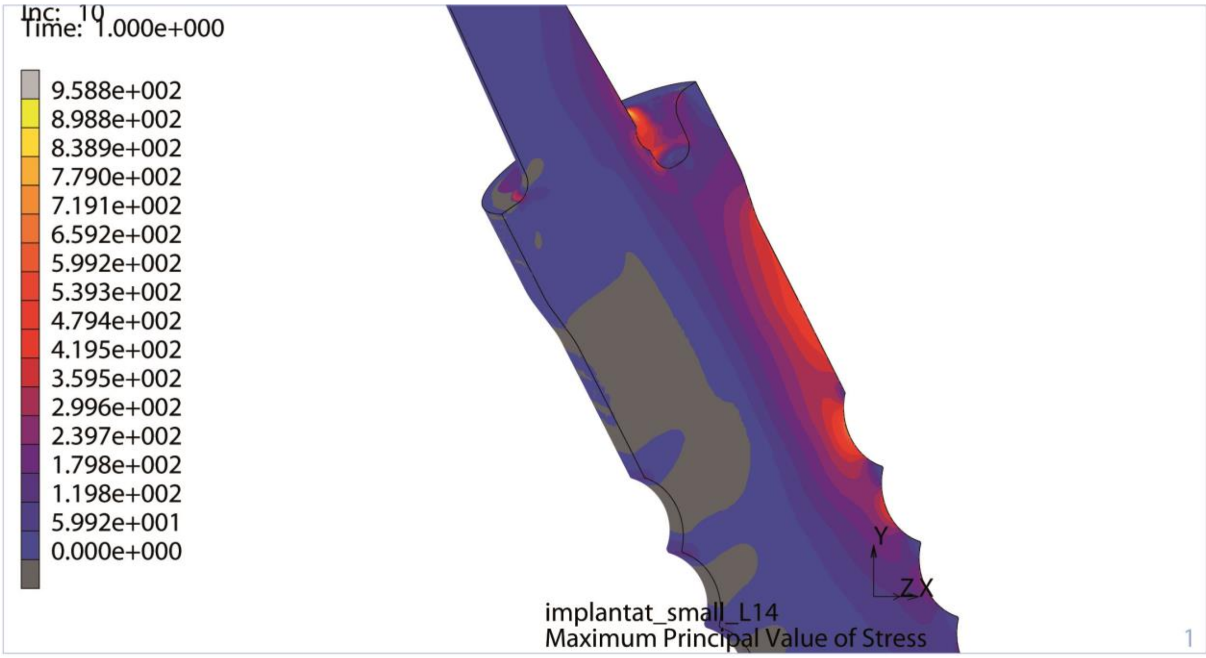

Fig. 25: Model 2 (-30°), load 200 N: Maximum principal stresses [MPa].

Model 2 (-30°): Vertical load 200 N

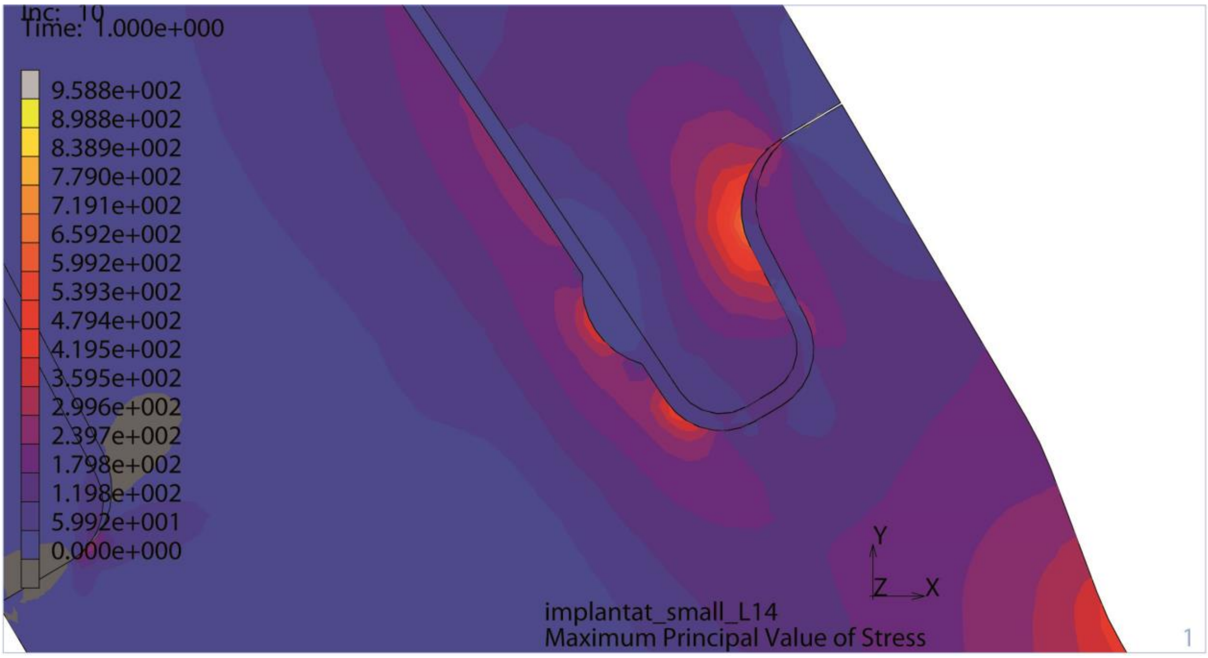

Fig. 26: Model 2 (-30°), load 200 N: Maximum principal stresses [MPa].

Model 3 (+30°): Vertical load 200 N

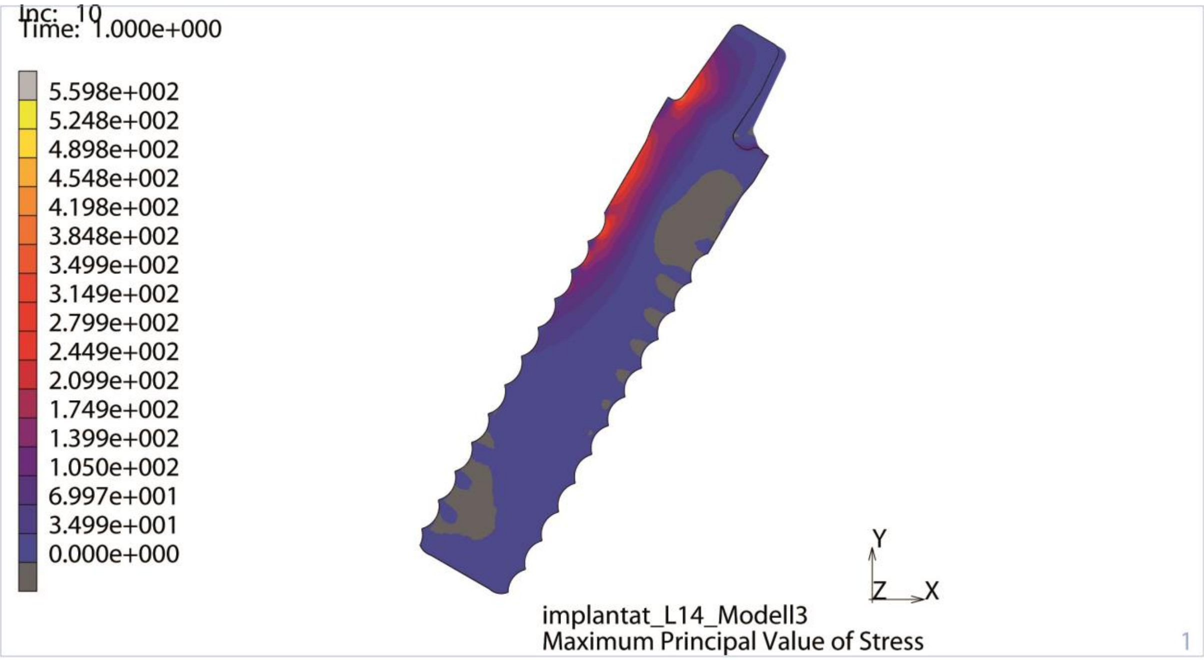

Fig. 27: Model 3 (+30°), load 200 N: Maximum principal stresses [MPa].

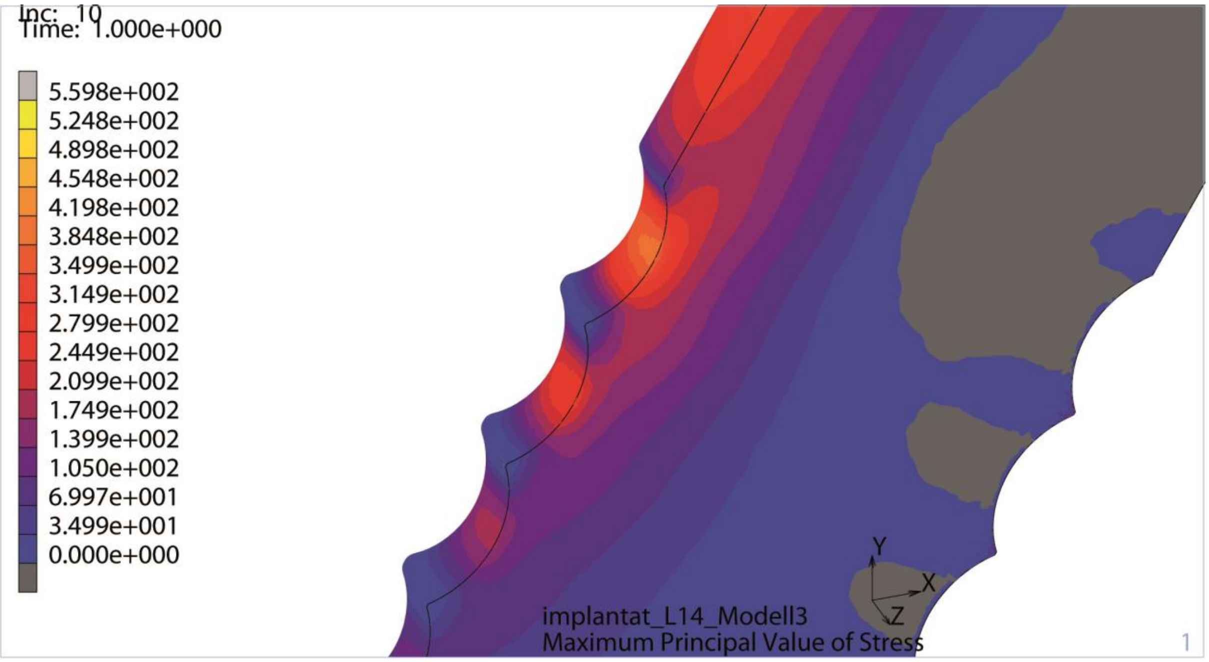

Fig. 28: Model 3 (+30°), load 200 N: Maximum principal stresses [MPa].

Model 3 (+30°): Vertical load 200 N

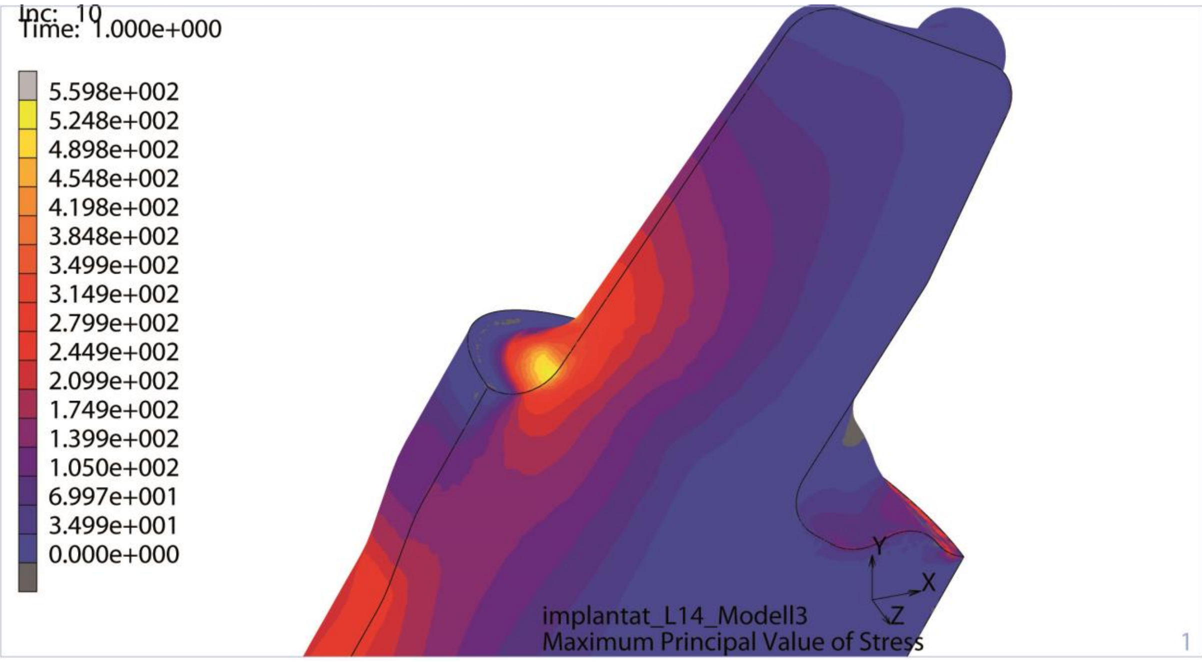

Fig. 29: Model 3 (+30°), load 200 N: Maximum principal stresses [MPa].

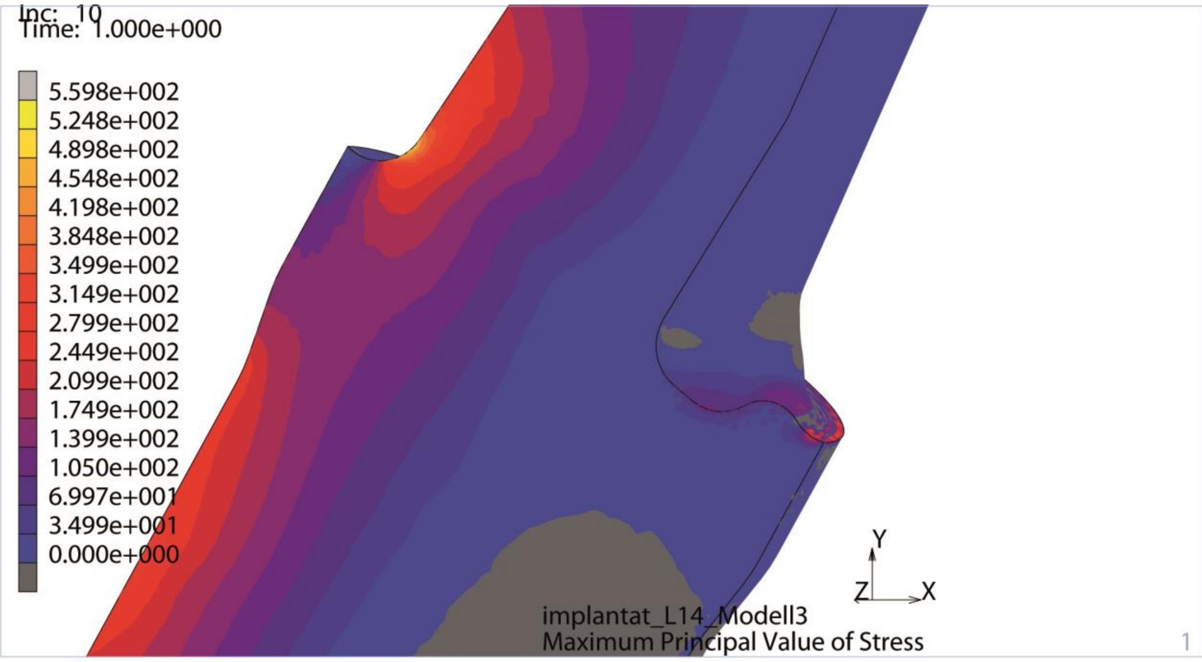

Fig. 30: Model 3 (+30°), load 200 N: Maximum principal stresses [MPa].

Model 3 (+30°): Vertical load 200 N

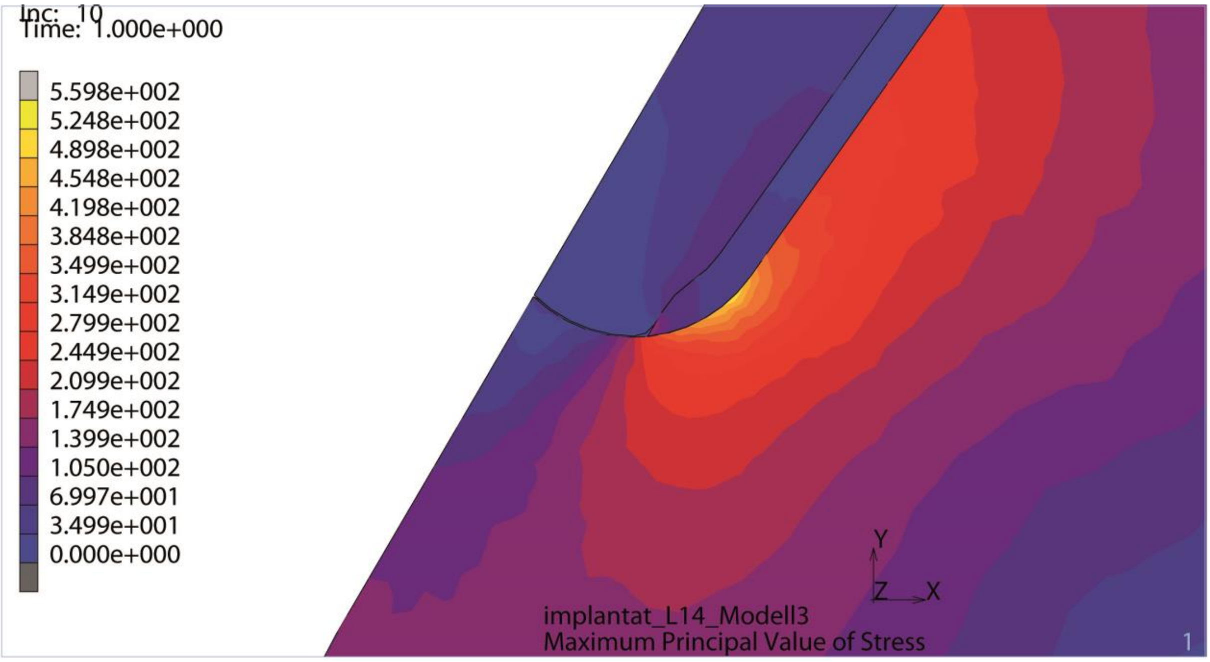

Fig. 31: Model 3 (+30°), load 200 N: Maximum principal stresses [MPa].